Evolving Imaging Model for Super-Resolution Reconstruction

Michal Kawulok
Future Processing / Silesian University of Technology
Gliwice, Poland
michal.kawulok@polsl.pl

Pawel Benecki
Future Processing / Silesian University of Technology
Gliwice, Poland
pbenecki@future-processing.com

Daniel Kostrzewa
Future Processing / Silesian University of Technology
Gliwice, Poland
daniel.kostrzewa@polsl.pl

Lukasz Skonieczny
Future Processing
Gliwice, Poland
lskonieczny@future-processing.com

ABSTRACT

Super-resolution reconstruction (SRR) allows for enhancing image spatial resolution from low-resolution (LR) observations, which are assumed to have been derived from a hypothetical high-resolution image by applying a certain imaging model (IM). However, if the actual degradation is different from the assumed IM, which is often the case in real-world scenarios, then the reconstruction quality is affected. We introduce a genetic algorithm to optimize the SRR hyper-parameters and to discover the actual IM by evolving the kernels exploited in the IM. The reported experimental results indicate that our approach outperforms the state of the art for a variety of images, including difficult real-life satellite data.

CCS CONCEPTS

• **Computing methodologies → Reconstruction**; **Genetic algorithms**; *Image processing*;

KEYWORDS

Super-resolution reconstruction, Genetic algorithm

ACM Reference Format:

Michal Kawulok, Pawel Benecki, Daniel Kostrzewa, and Lukasz Skonieczny. 2018. Evolving Imaging Model for Super-Resolution Reconstruction. In *GECCO '18 Companion: Genetic and Evolutionary Computation Conference Companion, July 15–19, 2018, Kyoto, Japan.* ACM, New York, NY, USA, Article 4, 2 pages. https://doi.org/10.1145/3205651.3205676

1 INTRODUCTION

Multiple-image super-resolution reconstruction (SRR) [7] allows for generating a high-resolution (HR) image from a set of N low-resolution (LR) observations: $\boldsymbol{I}^{(L)} = \{\mathcal{I}_i^{(l)} : i \in [1..N]\}$. The majority of the existing approaches employ a parametrized imaging model (IM) to simulate the process of degrading a hypothetical HR image $\mathcal{I}'^{(h)}$ into $\mathcal{I}^{(l)}$ (such IMs include warping, blurring, downsampling and contamination with the noise). SRR is aimed at inverting the IM to reconstruct $\mathcal{I}'^{(h)}$, which is an ill-posed optimization problem.

In [4], SRR is performed relying on image registration using iterative back-projection (IBP). A hierarchical subpixel displacement estimation is combined with the Bayesian reconstruction in the gradient projection algorithm (GPA) [6]. In [1], the subpixel registration parameters are determined with a genetic algorithm (GA), and regularization is ensured with certain constraints on the genetic operators. Projection onto convex sets [2] consists in updating $\mathcal{I}'^{(h)}$ iteratively based on the difference between $\mathcal{I}^{(l)}$ and $\mathcal{I}'^{(h)}$ degraded using the IM. Fast and robust super-resolution (FRSR) [3] measures the error in the HR coordinates, thus avoiding the expensive scaling operation. SRR for satellite images was proceeded using adaptive detail enhancement (SR-ADE) [8], which amplifies the high-frequency detail information. Evolutionary methods were used to reconstruct an HR image given a fixed IM, and in our earlier work [5] we optimized the FRSR hyper-parameters (GA-FRSR). However, evolution of the IM itself has not been considered so far.

Our contribution lies in proposing a new GA (EvoIM) to evolve the kernels of the IM exploited in the well-established FRSR method, alongside optimizing its hyper-parameters. This allows for adapting the IM to the actual degradation learned from a training set ($\boldsymbol{T}$).

2 EVOLVING THE IMAGING MODEL

In FRSR [3], the IM consists in the Gaussian blur ($\boldsymbol{B}$) followed by the decimation to obtain an LR observation. This process is inverted to reconstruct the HR image as a solution ($\mathcal{X}$) of the minimization problem, solved using the gradient descent with the update step:

$$\Delta\mathcal{X} = -\beta\left[\boldsymbol{B}'\boldsymbol{A}^T\operatorname{sgn}(\boldsymbol{A}\boldsymbol{B}\mathcal{X}_n - \boldsymbol{A}\mathcal{X}_0) + \lambda\frac{\delta U(\mathcal{X})}{\delta\mathcal{X}}(\mathcal{X}_n)\right], \quad (1)$$

where β controls the step length, $\boldsymbol{A}$ is a diagonal matrix of the LR contribution to $\mathcal{X}_0$ and $\boldsymbol{B}' = \boldsymbol{B}^T$ is the deconvolution of the Gaussian blur. $U(\mathcal{X})$ is the regularization term controlled with λ, and configured with two hyper-parameters: the spatial decay α ($0 < \alpha < 1$), and regularization shift size $P \in \{1, 2, 3\}$.

In EvoIM, we substitute the Gaussian blur in $\boldsymbol{B}$ and $\boldsymbol{B}'$ with two evolvable 5×5 convolution kernels—we assume they are symmetrical, hence each kernel is encoded using 6 numbers in the range $(-1; 1)$. These values, along with α, β, λ and P, form a 16-dimensional search space, traversed by our GA.

A population of $N_P = 10$ individuals is evolved using genetic operators (*selection*, *cross-over* and *mutation* with the probability $P_m = 0.2$), and the elitism is ensured. The fitness η is computed based on a training set $\boldsymbol{T}$, composed of several scenes—each scene contains an $\boldsymbol{I}^{(L)}$ set coupled with an HR ground-truth image $\mathcal{I}^{(h)}$.

GECCO '18 Companion, July 15–19, 2018, Kyoto, Japan

ACM ISBN 978-1-4503-5764-7/18/07.
https://doi.org/10.1145/3205651.3205676

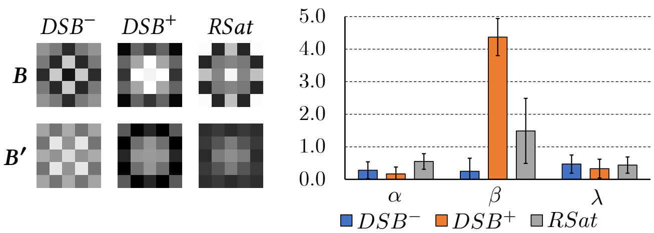

Figure 1: Examples of the optimized B and B' kernels (left) and the hyper-parameters values for different T's (right).

$\mathcal{I}'^{(h)}$ is reconstructed from $\boldsymbol{I}^{(L)}$ using FRSR (configured by the chromosome of the evaluated individual), and η is obtained as the structural similarity index (SSIM) between $\mathcal{I}^{(h)}$ and $\mathcal{I}'^{(h)}$, averaged for all the scenes in $\boldsymbol{T}$. We regenerate the population, if the average η does not increase in 3 generations.

3 EXPERIMENTAL VALIDATION

For validation, we used SPOT satellite images (100×100 pixels, 5 different scenes in $\boldsymbol{T}$ and the test set $\boldsymbol{\Psi}$), without (DSB^-) and with (DSB^+) Gaussian blur applied, each HR downscaled by a factor of 2 to obtain 4 different LR images. In a real-life scenario ($RSat$), we matched pairs of SPOT (HR) and Sentinel-2 (LR) images ($\boldsymbol{T}$ and $\boldsymbol{\Psi}$ include 10 HR images each of $317{\times}317$ and $211{\times}211$ pixels, matched with 5 LR 75×75 and 50×50 images). Every randomized method was run 30× on an Intel Xeon 3.2 GHz computer with 16 GB RAM (we implemented the algorithms in C++). Each test was given a time budget of 3600 seconds. We employed the two-tailed Wilcoxon test to verify whether the scores are significantly different.

In Figure 1, we show examples of the kernels (black: −1, white: 1) adapted to different variants of $\boldsymbol{T}$, and the obtained hyper-parameter values. For $RSat$, the values of α are significantly different from DSB^- and DSB^+ ($p < 0.001$), while they are not different between DSB^- and DSB^+ ($0.05 < p < 0.1$). The values of β are significantly different in all cases ($p < 0.001$), while λ's are different only between DSB^- and DSB^+ ($p < 0.05$). Overall, each degradation variant leads to a different set of kernels and hyper-parameter values.

The quantitative results are reported in Table 1 (for $RSat$, LR and HR images are acquired with different sensors, hence low SSIM scores). For EvoIM, we run a cross test between different variants of $\boldsymbol{T}$ and $\boldsymbol{\Psi}$ (the corresponding pairs are grayed). The scores for $\boldsymbol{\Psi}$ are very sensitive to the $\boldsymbol{T}$ used for training and EvoIM adapts well to the degradation model, much better than GA-FRSR which optimizes only hyper-parameters (we report the scores for the same variant of $\boldsymbol{T}$ and $\boldsymbol{\Psi}$). While there are no differences for DSB^-, the scores are significantly different for DSB^+ ($p < 0.001$) and $RSat$ ($p < 0.005$). For each of 3 variants of $\boldsymbol{\Psi}$, EvoIM outperforms the state of the art (for GA-SRR, $p < 0.001$). From an example of the qualitative results in Figure 2, it can be seen that EvoIM delivers visually best outcome and there is a noteworthy difference compared with GA-FRSR.

4 CONCLUSIONS

In this paper, we report our initial study on evolving the kernels for the IM used within a well-established FRSR technique. The reported experiments indicate that the proposed EvoIM algorithm successfully adapts the IM to the actual degradation (simulated or real), outperforming the investigated state-of-the-art methods.

Our ongoing work is on evolving larger kernels and other elements of the IM. We will also enhance the evaluation procedure to embrace several categories of real-world images, to verify whether and how the optimal kernels depend on the sensor type.

Table 1: SSIM scores for different variants of $\boldsymbol{T}$ and $\boldsymbol{\Psi}$, obtained using EvoIM and other SRR methods.

EvoIM		Variant of $\boldsymbol{\Psi}$		
$\boldsymbol{T}\downarrow$	η	DSB^-	DSB^+	$RSat$
DSB^-	.984 ± .001	**.977 ± .002**	.655 ± .005	.364 ± .019
DSB^+	.836 ± .002	.869 ± .015	**.818 ± .003**	.333 ± .024
$RSat$	.459 ± .002	.825 ± .020	.606 ± .021	**.428 ± .012**
	GA-FRSR [5]	**.977 ± .002**	.746 ± .002	.418 ± .012
	GA-SRR [1]	.875 ± .002	.621 ± .003	.410 ± .013
	GPA [6]	.937	.583	.404
	IBP [4]	.911	.614	.424
	SR-ADE [8]	.848	.603	.388

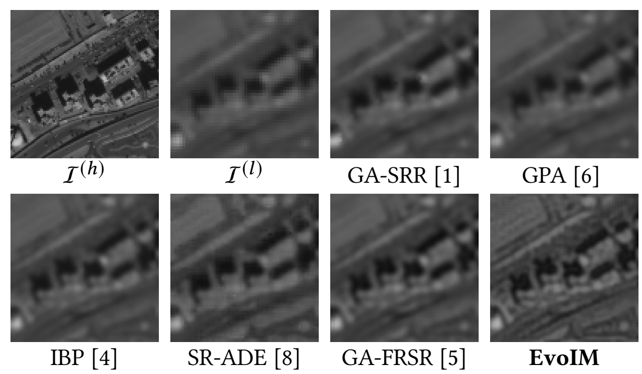

Figure 2: SRR outcome obtained with different techniques.

ACKNOWLEDGMENTS

The reported work was funded by European Space Agency (SISPARE project). Partial support by Institute of Informatics funds: BK-230/RAu2/2017 (MK) and BKM-509/RAu2/2017 (DK).

REFERENCES

[1] B. Ahrens. 2005. Genetic algorithm optimization of superresolution parameters. In *Proc. GECCO*. ACM, 2083–2088.

[2] T. Akgun, Y. Altunbasak, and R.M. Mersereau. 2005. Super-resolution reconstruction of hyperspectral images. *IEEE TIP* 14, 11 (2005), 1860–1875.

[3] S. Farsiu, M.D. Robinson, M. Elad, and P. Milanfar. 2004. Fast and robust multiframe super resolution. *IEEE TIP* 13, 10 (2004), 1327–1344.

[4] M. Irani and S. Peleg. 1991. Improving resolution by image registration. *CVGIP: Graphical Models and Image Process.* 53, 3 (1991), 231–239.

[5] M. Kawulok, P. Benecki, D. Kostrzewa, and L. Skonieczny. 2018. Towards Evolutionary Super-Resolution. In *Evostar 2018*. Springer, Cham, 480–496.

[6] R. Schultz and R. Stevenson. 1996. Extraction of high-resolution frames from video sequences. *IEEE TIP* 5, 6 (1996), 996–1011.

[7] L. Yue, H. Shen, J. Li, Q. Yuan, H. Zhang, and L. Zhang. 2016. Image super-resolution: The techniques, applications, and future. *Signal Process.* 128 (2016), 389–408.

[8] H. Zhu, W. Song, H. Tan, J. Wang, and D. Jia. 2016. Super resolution reconstruction based on adaptive detail enhancement for ZY-3 satellite images. *Proc. ISPRS Congress* (2016), 213–217.